

Classification of periodic and chaotic passive limit cycles for a compass-gait biped with gait asymmetries

Jae-Sung Moon[†] and Mark W. Spong^{‡*}

[†]*Department of Industrial and Enterprise Systems Engineering, University of Illinois at Urbana-Champaign, Urbana, IL 61801, USA*

[‡]*Department of Electrical Engineering, University of Texas at Dallas, Richardson, TX 75080, USA*

(Received in Final Form: February 16, 2011. First published online: March 23, 2011)

SUMMARY

In this paper we study the problem of passive walking for a compass-gait biped with gait asymmetries. In particular, we identify and classify bifurcations leading to chaos caused by the gait asymmetries because of unequal leg masses. We present bifurcation diagrams showing step period versus the ratio of leg masses at various walking slopes. The cell mapping method is used to find stable limit cycles as the parameters are varied. It is found that a variety of bifurcation diagrams can be grouped into six stages that consist of three expanding and three contracting stages. The analysis of each stage shows that marginally stable limit cycles exhibit period-doubling, period-remerging, and saddle-node bifurcations. We also show qualitative changes regarding chaos, i.e., generation and extinction of chaos follow cyclic patterns in passive dynamic walking.

KEYWORDS: Passive dynamic walking; Bifurcations and chaos; Gait asymmetries; Six stages of bifurcations; Composite hybrid systems.

1. Introduction

Passive dynamic walking refers to the property that a suitably designed biped can exhibit stable walking on a downhill slope without any actuation¹⁸ and is of great theoretical interest because of its several particular features. For example, passive walking is perfectly efficient since no external energy (other than gravity) needs to be supplied. Natural human walking is partly dependent on passive mechanism during the swing phase.^{19, 20} Passive dynamic walking also exhibits period-doubling bifurcations leading to a chaotic regime as the ground slope is varied.⁹

We are here interested in bifurcations and chaos obtained from changing parameters in the dynamic equations of passive walking. Goswami *et al.*¹⁰ used three parameters such as ground slope, leg masses, and positions of leg masses of a compass-gait biped. Changes in leg parameters were equally applied to both legs so that the biped showed symmetric walking until period-doubling bifurcations take place. After the bifurcations, no two steps are identical, but the irregular steps are periodically repeated. As the periodicity doubles, the walking gaits become more complicated and eventually

exhibit chaos where no steps are identical although the biped still walks stably. Since then, the same phenomenon has been observed from various walking models with different bifurcation parameters. Garcia *et al.*⁷ showed that a simplified walking model exhibits the same bifurcations in passive walking by plotting stance leg angles with increase in ground slopes. Aoi and Tsuchiya¹ used the simplest walking model driven by open loop sinusoidal inputs. Angular velocity of the input phase was used as one of the bifurcation parameters, and the authors¹ plotted phase of the oscillator at impact. Asano and Luo² used an underactuated biped with a torso and semicircular feet driven by the pseudo virtual passive dynamic walking method. Various outputs, including step periods, were plotted in terms of torso length as a bifurcation parameter. All the above studies on different systems have verified the occurrence of period-doubling bifurcations and chaotic attractors. In addition, Howell and Baillieul¹⁴ found not only period-doubling but also saddle-node bifurcations in a torso-driven biped with increase in torso lengths.

Bifurcations and chaos are of importance for further studies on passive dynamic walking. Suzuki and Furuta²⁸ investigated a chaos control to enlarge basins of attraction of passive walking using the so-called OGY (Ott–Grebogi–Yorke) method.^{23, 25} Kruz and Stergiou¹⁷ showed that hip actuation by a torsional spring can drive a passive dynamic walker from chaotic to periodic gaits. Recently, Asano and Luo³ studied walking efficiency related to bifurcations. Harata *et al.*¹² showed that the gait efficiency can be improved by changing the periodic gaits from period-2 to period-1 gaits using delayed feedback control.

All the above studies on bifurcations and chaos in passive or semi-passive dynamic walking have used symmetric models with two identical legs. A study of gait asymmetries could enhance our understanding of bipedal locomotion in both robots and humans, for instance, a better understanding of asymmetric walking for people with prosthetic limbs, injuries, surgical procedures, or disabilities that introduce asymmetries. Some control authority could be developed based on the results to compensate for disparities in legs and to generate balanced and symmetric walking gaits from gait asymmetries. Ephanov and Hurmuzlu⁵ showed that swing phase control can generate normal gaits of planar five-link biped with gait asymmetries.

In the following sections, we introduce a compass-gait biped with different leg masses and derive the equations

* Corresponding author. E-mail: mspong@utdallas.edu

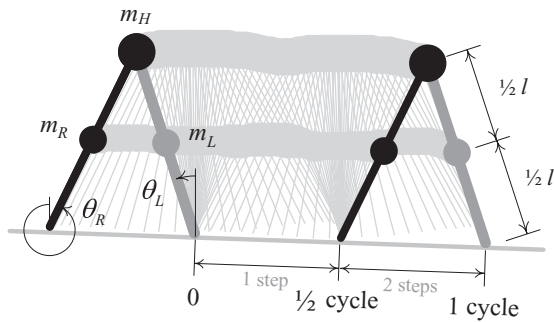


Fig. 1. A compass-gait biped and its one complete cycle of bipedal walking.

of motion. We then present a concept of composite hybrid systems that is a prerequisite for the analysis of asymmetric walking. The effects of gait asymmetries on passive walking are then investigated by computing bifurcation diagrams showing step periods versus two bifurcation parameters, which are the ground slope and the ratio of leg masses.

2. Model Description

2.1. Compass-gait bipeds with asymmetries

The compass-gait biped¹⁰ shown in Fig. 1 is used in this paper to investigate gait asymmetries. This two-degree-of-freedom biped has a hip joint connecting two straight legs and walks passively in the sagittal plane. There are no knees or a torso. A hip mass, m_H , is at the hip joint and two leg masses, m_L and m_R , are at the centers of left and right legs whose length is equal to l . Asymmetric walking is embodied by making one leg slightly longer or heavier than the other. In this paper, we primarily focus on bipeds with equal leg lengths but different leg masses. However, we have observed similar results to those presented here for the compass-gait biped with unequal leg lengths.

The movement of a compass-gait biped is divided into a swing phase and an impact phase. Since there is no external force, the total energy of the biped is conserved between impacts. The impact phase describes the instant when the swing leg strikes the ground after passing the stance leg. When the two legs are overlapped during the swing phase, the swing leg also scuffs the ground, but we ignore this touchdown in simulation. Knees or nonzero feet are required to avoid the scuffing in practice. We make standard assumptions that the impact is perfectly inelastic and there is no slipping at the stance foot/ground contact.¹⁶ In passive walking the loss of kinetic energy because of impact is compensated by the increment of potential energy gained from the change in the reference frame after impact.

2.2. Equations of motions

The equations of motion during the swing phase can be derived from the Lagrangian dynamics. We choose two leg angles θ_L and θ_R as generalized coordinates for the compass-gait biped. These angles are with respect to the vertical to level ground. It is important to note that gait asymmetry requires two distinct equations of motions: one for movement

with a left stance leg and the other for movement with a right stance leg. Gait asymmetry causes each movement to generate different trajectories, and thus the two equations of motions are alternately solved. Since the biped walks in the sagittal plane, we cannot distinguish between left and right legs. We designate the stance leg of the first step as the left leg, which becomes the swing leg of the second step. The dynamic equations²⁶ for the compass-gait biped with a left stance leg are described by

$$\begin{bmatrix} M_{11} & M_{12} \\ M_{21} & M_{22} \end{bmatrix} \ddot{q} + \begin{bmatrix} 0 & C_{12} \\ C_{21} & 0 \end{bmatrix} \dot{q} + \begin{bmatrix} G_1 \\ G_2 \end{bmatrix} = 0, \quad (1)$$

where $q = [q_L, q_R]^T = [\theta_L(t), \theta_R(t)]^T$, and

$$\begin{aligned} M_{11} &= l^2(4m_H + m_L + 4m_R)/4, \\ M_{12} &= M_{21} = -l^2 m_R \cos(q_L - q_R)/2, \\ M_{22} &= l^2 m_R/4, \\ C_{12} &= -C_{21} = -l^2 m_R \sin(q_L - q_R) \dot{q}_R/2, \\ G_1 &= -gl(2m_H + m_L + 2m_R) \sin(q_L)/2, \\ G_2 &= glm_R \sin(q_R)/2. \end{aligned}$$

The other dynamic equations with a right stance leg can be derived in a similar way.

Impact dynamics are governed by the conservation of angular momentum. Two distinct impact maps are also required because of the different masses of the impacting legs. One of the equations of motions is given as

$$\dot{q}^+ = R_L(q^-) \dot{q}^-, \quad (2)$$

where superscripts $-$ and $+$ denote variables just prior to and just after impact, respectively. The impact map⁹ with a left stance leg is described by

$$R_L(q^-) = \begin{bmatrix} r_{11}^+ & r_{12}^+ \\ r_{21}^+ & r_{22}^+ \end{bmatrix}^{-1} \begin{bmatrix} r_{11}^- & r_{12}^- \\ r_{21}^- & 0 \end{bmatrix}, \quad (3)$$

where

$$\begin{aligned} r_{11}^+ &= l^2(4m_H + 4m_L + m_R - 2m_L \cos(q_L^- - q_R^-))/4, \\ r_{12}^+ &= l^2 m_L (1 - 2 \cos(q_L^- - q_R^-))/4, \\ r_{21}^+ &= -l^2 m_L \cos(q_L^- - q_R^-)/2, \\ r_{22}^+ &= l^2 m_L/4, \\ r_{11}^- &= l^2(-m_L + 2(2m_H + m_L + m_R) \cos(q_L^- - q_R^-))/4, \\ r_{12}^- &= -l^2 m_R/4, \\ r_{21}^- &= -l^2 m_L/4. \end{aligned}$$

Another impact map with a right stance leg can be similarly derived.

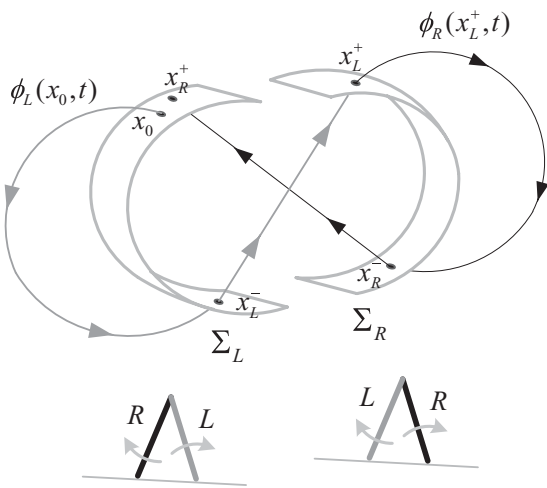


Fig. 2. Hybrid flows of a composite hybrid system. One walking cycle is represented by two continuous trajectories and two discrete jumps combining two distinct switching surfaces.

3. Methods

3.1. Hybrid flows of composite hybrid systems

One walking step has two phases: a continuous swing phase and a discrete impact phase. This type of a dynamic system is said to be a hybrid system. Let $q_L, \dot{q}_L, q_R, \dot{q}_R$ be state variables denoted by $x \in \mathbb{R}^4$, then state equations of each phase are given by $\dot{x} = f(x)$ and $x^+ = h(x^-)$, respectively. $f(\cdot)$ and $h(\cdot)$ with a left stance leg can be derived from Eqs. (1) and (2).

In the case of walking with gait asymmetry it is necessary to distinguish two terms, cycle and step. One walking cycle with gait asymmetry consists of two steps as shown in Fig. 1. Therefore, its dynamics requires four state equations, which are as follows:

$$H_L : \begin{cases} \dot{x} = f_L(x), & x \notin \Sigma_L, \\ x_L^+ = h_L(x_L^-), & x \in \Sigma_L, \end{cases} \quad (4)$$

$$H_R : \begin{cases} \dot{x} = f_R(x), & x \notin \Sigma_R, \\ x_R^+ = h_R(x_R^-), & x \in \Sigma_R. \end{cases} \quad (5)$$

The two hybrid systems H_L and H_R for left and right stance legs represent a composite hybrid system. Σ_L and Σ_R are switching surfaces where a swing leg is in contact with the ground.

Fig. 2 illustrates hybrid flows of a four-dimensional composite hybrid system or asymmetric walking trajectories of a compass-gait biped. The continuous flow $\phi(x, t)$ is a solution to the continuous dynamics $f(x)$, and two discrete flows from $h(x^-)$ combine the two switching surfaces. A trajectory starting at an initial condition $x_0 \in \Sigma_L$ returns to Σ_L at x_L^- just before the right swing leg hits the ground. After touchdown, the trajectory instantaneously jumps to $x_L^+ \in \Sigma_R$ at which the second step starts. In a similar fashion, the trajectory returns to Σ_L again completing one walking cycle at x_R^+ that will be an initial condition for the next walking cycle. If a biped has symmetric legs, then both switching surfaces are equivalent and one walking step is equal to one walking cycle.

3.2. Poincaré map method

We consider two hyperplanes $\tilde{\Sigma}_L$ and $\tilde{\Sigma}_R$ that are three dimensional and transversal to the flow $\phi(x, t)$ of continuous solutions. When a biped walks on a slope that has a fixed angle of inclination, one leg angle is dependent on the other leg angle if both legs are on the switching surface. Thus, these hyperplanes are induced by subtracting one dimension corresponding to a leg angle from the switching surfaces Σ_L and Σ_R . Let $x_i \in \mathbb{R}^3$ denote a state variable x on $\tilde{\Sigma}_L$ after completing i cycles. If we select a hyperplane $\tilde{\Sigma}_L$ as a Poincaré section on which a closed orbit hits every cycle, then the Poincaré map P is a mapping from $\tilde{\Sigma}_L$ to $\tilde{\Sigma}_R$ to $\tilde{\Sigma}_L$ again, and can be defined by

$$x_{i+1} = P(x_i), \quad (6)$$

where $P : \tilde{\Sigma}_L \rightarrow \tilde{\Sigma}_L$.²⁷ P is obtained by using the state variable x_i numerically updated from Eqs. (4) and (5) for every other hyperplane.

A walking cycle satisfying $x^* = P^k(x^*)$ is called a period- k motion, which means $x_{i+k} = x_i$, and the hybrid flows form a limit cycle. k is said to be the periodicity of the limit cycle, which has k fixed points on the Poincaré section. The stability of the limit cycle is determined by using the Jacobian of the Poincaré map near the fixed points.^{7, 10} If the eigenvalues of the linearization lie in the unit circle, then the closed orbit is locally asymptotically stable.

We use the Newton–Raphson algorithm to find the period- k fixed points. The following iterative process makes a good initial guess rapidly converge to either stable or unstable fixed points.²⁴

$$x_{i+k} = x_i - (D_x H(x_i))^{-1} \cdot H(x_i), \quad (7)$$

where $H(x_i) = P^k(x_i) - x_i$ and D_x is the Jacobian of a function.

3.3. Cell mapping method

We use the cell mapping method¹⁵ to find stable limit cycles of composite hybrid systems and their periodicities. A feasible region $\mathcal{F} \subset \tilde{\Sigma}_L$ containing a given initial condition x_0 as a starting point of the cell mapping process is minced into a large number of small cell cubes. x_0 is the location of the cell cube placed at the center of \mathcal{F} . $Va(\cdot)$ indicates the value of the cell cube that contains its state variable. Before mapping, all $Va(\cdot)$ are initialized to -1 indicating that all cell cubes are virgin cells except for one that contains x_0 . We set $Va(x_0) = 0$. The mapping process starts from x_0 and proceeds forward using Poincaré mapping such as

$$x_0 \rightarrow P(x_0) \rightarrow P^2(x_0) \rightarrow \dots \rightarrow P^i(x_0). \quad (8)$$

At each step in generating this sequence, we need to consider the following:

1. If a cell cube containing a newly generated $P^i(x_0)$ is a virgin cell, which means $Va(P^i(x_0)) = -1$, then we set $Va(P^i(x_0)) = i$, and carry out the next mapping.
2. In case a newly generated $P^i(x_0)$ is outside of \mathcal{F} , the original cell mapping method puts it into a sink cell

and terminates the sequence. We, however, ignore this mapping and go on to next mapping since the state variable comes back into \mathcal{F} as long as the flow is stable.

3. $Va(P^i(x_0)) \geq 0$ indicates that the current cell cube has encountered one of the previous sequences, and the current sequence has converged to a limit cycle. Now, this process is terminated. Suppose that the number of the cycle at this moment is n , the periodicity k of the limit cycle is given by

$$k = n - Va(P^n(x_0)). \tag{9}$$

When it comes to practical considerations, the accuracy of convergence can be improved by reducing the size of cell cubes, but the smaller size of cell cubes yields larger computation time. As for the feasible region \mathcal{F} , it is hard to choose sufficiently large \mathcal{F} such that $x^* \in \mathcal{F}$ in the beginning. If a flow does not come back to \mathcal{F} in an appropriate number of cycles, then x_0 should be placed at the current state variable and another mapping process resumes in $\mathcal{F}_{new} \subset \tilde{\Sigma}_L$ until the flow converges to a fixed point.

In the following section, we investigate bifurcation diagrams. In order to plot them, we need to find all fixed points as system parameters are varied. The current fixed point can be used as an initial condition to find next one based on the inference that if changes in parameters of the system are sufficiently small, then a fixed point of a limit cycle can still remain in the basin of attraction. The changes will lead the current fixed point to another one incorporated in a new limit cycle as system dynamics evolves.

4. Bifurcation Diagrams

We consider a compass-gait biped with different leg masses. Thus, bifurcation diagrams can be drawn by two bifurcation parameters, the ground slope and the ratio of leg masses. As parameters of equations of motions are varied, bifurcations may occur in the qualitative structure of the solutions.¹¹ In bipedal locomotion, the bifurcations are observed from some properties of walking cycles such as step period, walking speed, double-support angles between two legs, and so on. As seen in the previous studies, changes in the ground slope give rise to period-doubling bifurcations leading to chaos. Variations in leg masses also cause bifurcations, and thus mass ratio $r_m = m_R/m_L$ can be another bifurcation parameter. $r_m = 1$ means that both legs are the same.

4.1. Previous studies on passive walking with symmetric legs

Our numerical simulations for passive walking with two identical legs also verified the appearance of the period-doubling bifurcations in passive walking with increase in the ground slopes.⁸ System parameters were set to $m_H = 10$ kg, $m_L = m_R = 5$ kg, and $l = 1$ m, which appeared in Goswami *et al.*⁸ Figs. 3 and 4 represent bifurcation diagrams showing periods of each step in terms of the ground slope. In Fig. 3, solid lines are stable gaits, and dotted lines are unstable gaits obtained using the Newton–Raphson algorithm. Lines 1 and 2 indicate the unstable period-1 gaits, and Line 3 indicates the unstable period-2 gait. There are also unstable period-4

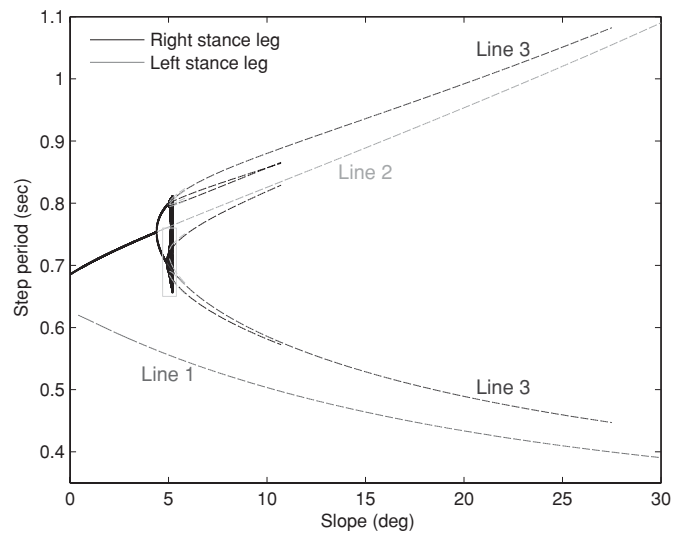


Fig. 3. Symmetric walking at various ground slopes.

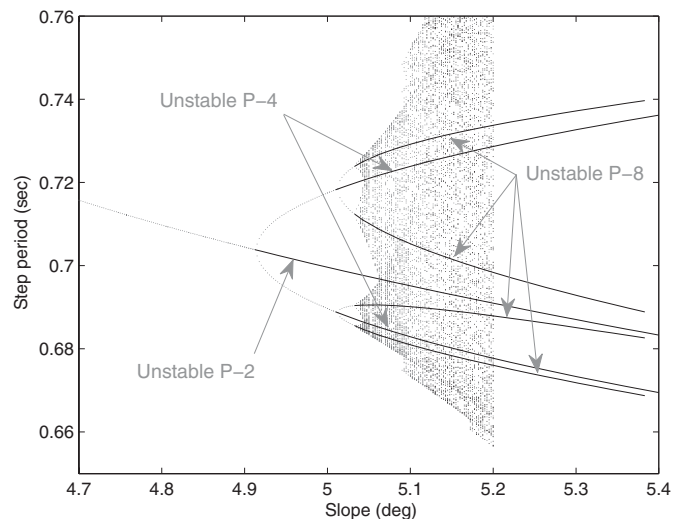


Fig. 4. A magnified diagram showing the inside of gray box in Fig. 3.

and period-8 gaits that are clearly seen as the solid lines in Fig. 4. Stable gaits exist in the shallow slopes in contrast to the range of the unstable gaits. According to our simulation results, the lowest slope at which the stable passive walking exists is 0.03° , and the highest slope is 5.20° .

Fig. 4 shows the route to chaos through period-doubling bifurcations. The diagram starts from the stable period-2 gait since the first period-doubling bifurcation already occurred at the 4.38° slope. As the slope increases, the stable period-2 gait turns into the unstable period-2 gait above 4.92° , and simultaneously gives rise to the new stable period-4 gait. Now there exist four gaits that include one stable period-4 gait and three unstable gaits such as two unstable period-1 gaits and one unstable period-2 gait. In a similar manner, the stable period-4 gait turns into the unstable period-4 gait above 5.01° and the new stable period-8 gait simultaneously takes place. This process is repeated until chaos occurs. We could not numerically find unstable period-16 gaits using the Newton–Raphson algorithm.

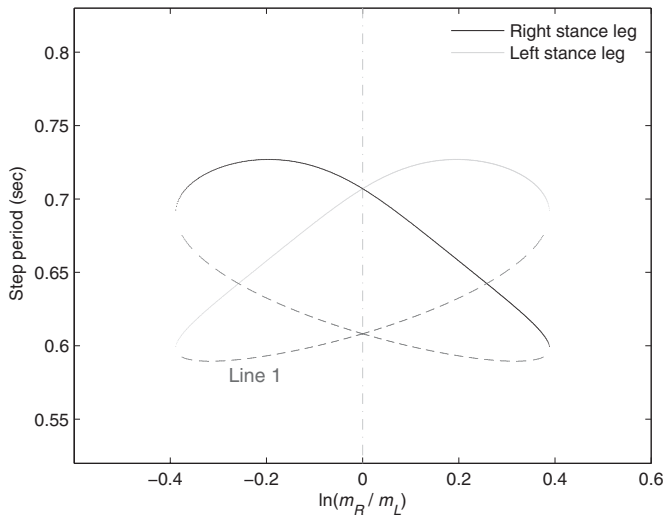


Fig. 5. Asymmetric walking at a 1.20° slope.

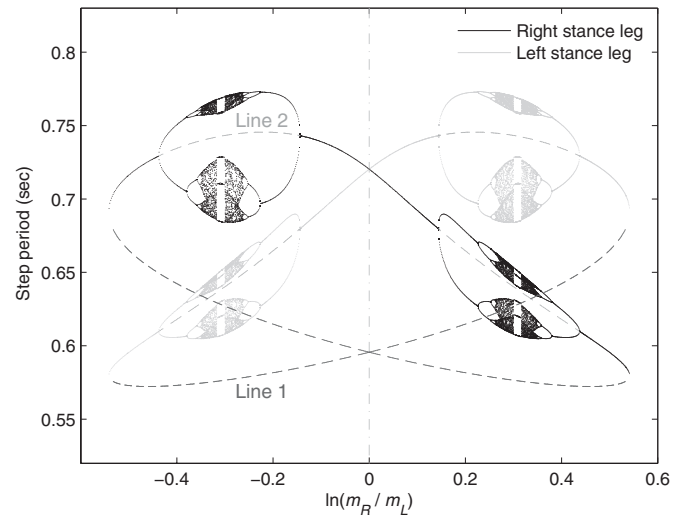


Fig. 6. Asymmetric walking at a 2.04° slope.

4.2. Bifurcation diagrams in gait asymmetries

We performed numerical simulations for a compass-gait biped with asymmetric legs. All parameters except for r_m were fixed as follows: $m_H = 10$ kg, $m_{leg} = m_L + m_R = 10$ kg, $l = 1$ m. Although r_m is varied, the total mass of the system is constant at 20 kg since the sum of the two leg masses was fixed. As for the cell mapping method, the length of one side of a small cell cube was set to 10^{-8} and the feasible region was composed of $100 \times 100 \times 100$ cubes.

We calculated walking periods that elapse between Poincaré sections and the moduli of the eigenvalues of the Jacobian of Poincaré maps as a function of r_m . Figs. 5 and 6 show bifurcation diagrams plotted in the logarithmic x-axis at 1.20° and 2.04° slopes, respectively. The vertical axes indicate walking periods. Instead of plotting a cycle period, we divided it into two-step periods for left and right stance legs. We chose $\tilde{\Sigma}_L$ as the Poincaré section and thus the trajectory hits $\tilde{\Sigma}_L$ at every two steps. Thus, in view of step periods, period-1 gaits look like period-2 gaits. Lines 1 and 2 indicate likewise unstable period-1 gaits.

Fig. 5 clearly shows saddle-node bifurcations. At $\ln r_m = 0$, a stable period-1 gait and an unstable period-1 gait are exhibited. As $\ln r_m$ increases, the former becomes less stable and the latter becomes less unstable because of the following reason: When we look at the magnitudes of the eigenvalues of the Jacobian of the Poincaré map, the maximum modulus of the stable gait begins to increase toward the boundary of the unit circle, but those of the unstable gait, already being out of the unit circle, decreases toward the unit circle. Both gaits come together at $\ln r_m = 0.3887$ where a saddle-node is located. There exist no gaits beyond 0.3887. As $\ln r_m$ decreases in the opposite direction, bifurcations symmetric about $\ln r_m = 0$ take place. This symmetric property means that the walking gaits are invariant even if both leg masses are exchanged with each other.

In addition to the saddle-node bifurcations, Fig. 6 shows period doubling and period remerging,⁴ like retro-doubling bifurcations satisfying the Feigenbaum constant⁶ in passive walking.^{7,21} At $\ln r_m = 0.0000$ to 0.1432, a period-1 gait appears. Two-step periods are equal at $\ln r_m = 0$, but they

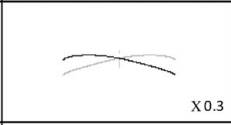
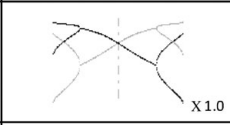
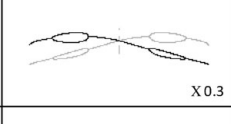


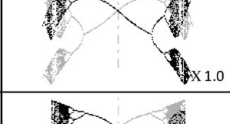
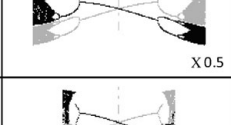
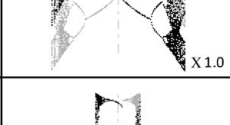
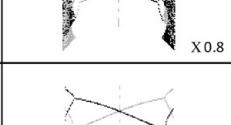



diverge when two legs have different masses that causes the so-called limping walk, so that one leg moves for longer time than the other one because of the gait asymmetry. A period-2 gait appears when $\ln r_m$ is greater than 0.1432, and the periodicity is doubled as $\ln r_m$ increases until chaos appears. We note that changes in the periodicities of both legs are exactly concurrent. As $\ln r_m$ increases farther, chaotic attractors are suddenly contracted and expanded making windows of chaos, which is called the interior crisis,²² and period remerging occurs to make the trajectories converge into a period-1 gait. These walking gaits are terminated at $\ln r_m = 0.5412$ where a saddle-node is located. The biped no longer walks stably beyond this point and falls over.

4.3. Cyclic streams of bifurcation diagrams

We continued to examine bifurcation diagrams of asymmetric legs by changing slopes from 0.03° to 5.20°. As results, we discovered cyclic streams of bifurcations within these ranges, and each slope had its own bifurcation diagram that could be classified as one of the six distinct stages according to their shape of stable walking gaits as shown in Table I. The six stages are named from A to F, respectively, and there are two sets of six stages since they are cyclic. The first set of six stages denoted by 1 comes to an end at a 2.95° slope, after which the second set of six stages denoted by 2 starts. The bottom right corner indicates the magnification of the diagrams. In A1, for instance, 0.3 means that the diagram was reduced to 30% of its original size. The gray dotted lines that cross the center of the diagrams indicate $\ln r_m = 0$, i.e., walking gaits with symmetric legs.

The bifurcation diagram of the symmetric legs can be reconstructed out of the diagrams of the asymmetric legs by extracting the points on the gray dotted lines. If all these points were put together, the resulting diagram would be identical with the diagram of stable gaits as given in Fig. 3 that looks like one of the diagrams in stage D. Stable period-1 gaits appear from A1 to D2 at $\ln r_m = 0$ with increase in slopes. Then stable period-2 gaits appear in E2 at $\ln r_m = 0$. They are still period-1 gaits in a composite hybrid system, but period-2 gaits for a biped with symmetric legs that

Table I. Six stages of bifurcation diagrams.

Stage Slope	Bifurcation diagrams Period vs. Mass ratio r_m	Stage Slope	Bifurcation diagrams Period vs. Mass ratio r_m
A1 0.80°	 X0.3	A2 3.50°	 X1.0
B1 1.90°	 X0.3	B2 3.60°	 X1.0
C1 2.04°	 X0.3	C2 3.74°	 X1.0
D1 2.10°	 X0.5	D2 3.80°	 X1.0
E1 2.74°	 X0.8	E2 4.70°	 X1.0
F1 2.95°	 X1.0	F2 4.96°	 X1.0

has only one switching surface. In this way, period-4 gaits appear in stage F2. As the slope increases, the diagram in F2 moves to the right-hand side, which causes period-doubling bifurcations at $\ln r_m = 0$. Finally, this process comes to an end at a 5.20° slope without period-remerging bifurcations.

In the following section, we describe the features of each stage. It is known that period-doubling gaits take place at the moment when the eigenvalues of the Jacobian of the Poincaré map hit the boundary of the unit circle. Thus, we examine each stage by focusing on the stability of stable walking gaits using the eigenvalues.

5. Six Stages of Bifurcations

5.1. Stage A

Bifurcation diagrams begin to expand from stage A where no bubbles appear until the next stage B as shown in Table I. The ranges of stage A1 and A2 are from 0.03° to 1.75° and 2.96° to 3.55° slopes, respectively. As seen in the Section 4.2, saddle-node bifurcations were observed, and thus the tips of diagrams are connected with unstable gaits in not only A1 but also in B1 and C1 where the diagrams of these three stages expand. As for the saddle-node bifurcations in A2, we could not have enough information from numerical simulations.

The diagram of stage A expands with increase in the slope. In case of stage A1 there are no changes in periodicities of stable gaits, but the stability of the system is getting worse because the eigenvalues are approaching the boundary of the unit circle as shown in Figs. 7(a) and (b). The arrows illustrate the direction of the movement of the eigenvalues as the slopes increase. The upper diagram shows step periods in terms of $\ln r_m$, and the lower diagram indicates moduli of the eigenvalues ranging from zero to one since only stable gaits were plotted. The moduli of unstable gaits are always bigger than one. The moduli of the eigenvalues begin to swell around midpoints between $\ln r_m = 0$ and both tips as shown in Fig. 7(b), and Fig. 7(c) finally shows that bubbles are formed at the place where the peak of the hump touches one. A2 in Table I already shows stable period-2 gaits because of period-doubling bifurcations, but there is no occurrence of bifurcations until increasing slopes make bubbles.

5.2. Stage B

Once bubbles have been formed, child bubbles are formed inside the bubbles, and then grandchild bubbles are consecutively formed in the child bubbles while diagrams are expanding with increasing slopes. Stage B is described by this spawning before chaos appears in the next stage C. The ranges of stages B1 and B2 are from 1.76° to 2.01° and 3.56° to 3.69° slopes, respectively.

In Fig. 7(c), the most fragile regions are located at around $r_m = 0.75$ and 1.31 where the first bubbles appeared as results of successions of two different types of bifurcations.

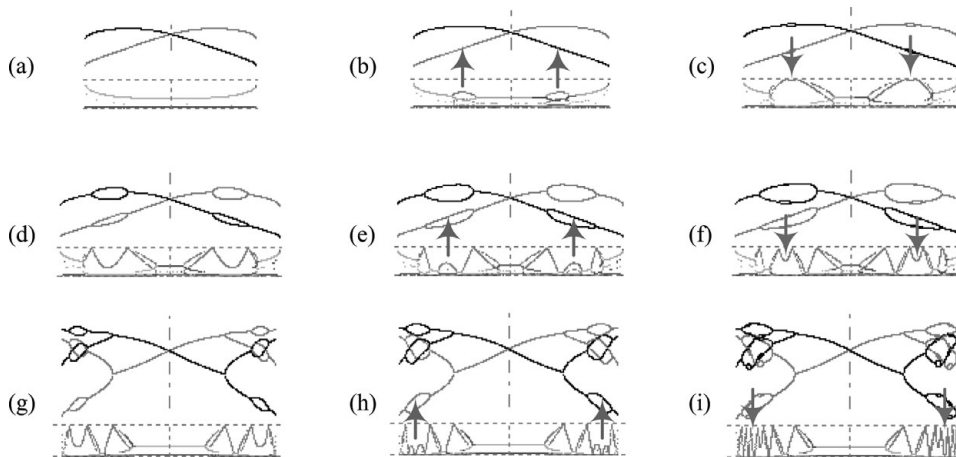


Fig. 7. Bifurcation diagrams at different slopes and the corresponding magnitudes of the eigenvalues of the Jacobian of the Poincaré map in stages A and B: (a) 1.20° slope, (b) 1.52° slope, (c) 1.76° slope, (d) 1.84° slope, (e) 1.92° slope, (f) 1.98° slope, (g) 3.60° slope, (h) 3.64° slope, and (i) 3.68° slope.

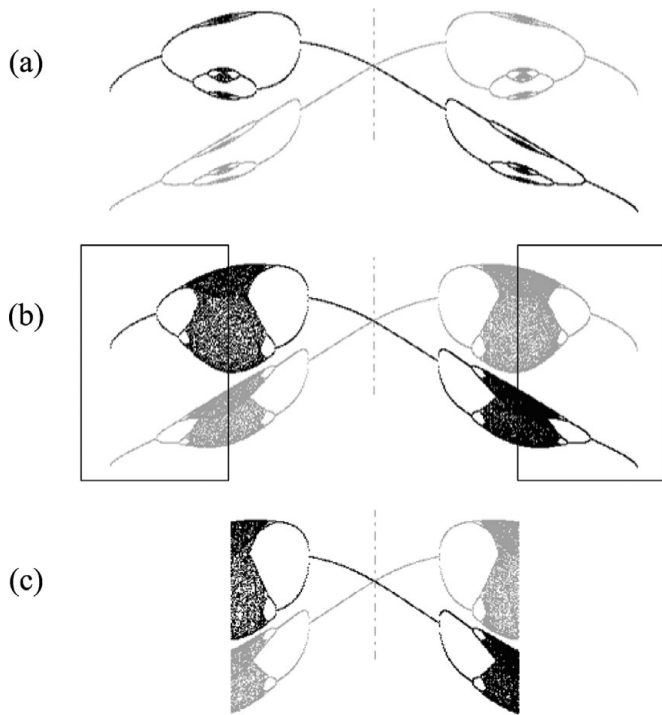


Fig. 8. Transitions from stage C1 to D1: (a) 2.02° slope, (b) 2.09° slope, and (c) 2.10° slope.

One is period-doubling bifurcations, and the other is period-remerging bifurcations. Bier and Bountis⁴ called them the period-bubbling bifurcation as a whole. After bubbles are formed, they grow and get stabilized since the eigenvalues of the interiors of the bubbles return back toward zero as shown in Fig. 7(d). With increasing slopes, new humps come out from the fully stabilized eigenvalues, and they are rising again as shown in Fig. 7(e). Finally, the humps yield child bubbles and period-4 gaits shown in Fig. 7(f). In this way consecutive child bubbles are created by new born humps from the parent bubbles. As for the movement of the humps, only one dominant eigenvalue goes back and forth along the real axis.

It is observed that the first bubble in B1 gives birth to one child bubble, but those in B2 simultaneously bears two child bubbles formed in each branch of the first bubble because two humps of eigenvalues rise at the same time from the bottom as shown in Figs. 7(g), (h), and (i).

5.3. Stage C

Chaos appears in stage C as shown in C1 and C2 of Table I. The ranges of stages C1 and C2 are from 2.02° to 2.09° and 3.70° to 3.74° slopes, respectively. Bifurcation diagrams are still expanding and being filled with chaos with increase in slopes. Walking gaits are stable in chaos, but we are not able to analyze the stability using eigenvalues, since there are no more fixed points on the Poincaré section. In fact, it is hard to tell the difference between high periodic gaits and chaos based on numerical results. The Lyapunov exponent is used to numerically analyze the chaotic attractor,¹³ but we did not go further to analyze the chaos.

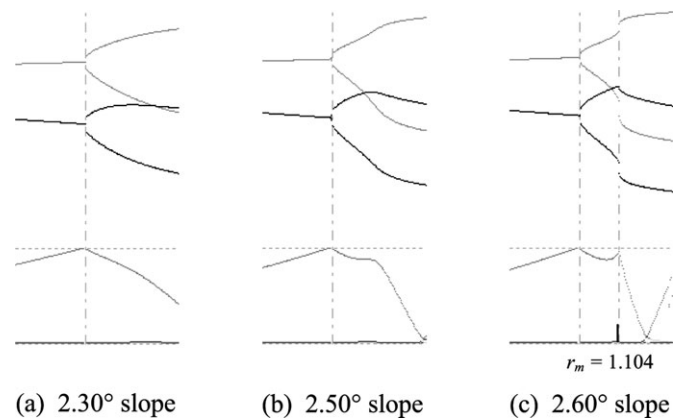


Fig. 9. Transitions in stage E1.

5.4. Stage D

The previous three stages have been expanding so far with increasing slopes. Stage D is a turning point at which bifurcation diagrams begin to contract, and the diagrams of the following stages E and F also contract. At the end of stage C, the first born bubbles are full of chaos. A slight increment of slope causes the extinction of outermost remerged parts, including chaos, and then bifurcation diagrams are contracting as slopes increase. Fig. 8 shows the process. Fig. 8(a) is an incipient diagram of stage C1 where chaos is distributed over narrow areas. Fig. 8(b) is the last moment of the stage and filled with chaos. The transition from Figs. 8(b) to (c) is triggered by a 0.01° slope, and then both ends in the boxes vanish instantly. Stages D1 and D2 of Table I seem to have only period-doubled regions because period remerged parts vanish away.

When it comes to the range of stage, we do not identify them from here because the three contracting stages exhibit three distinct changes of bifurcation diagrams. We are here more concerned with the qualitative changes than the ranges of stages, which can be divided into two parts by a disconnection point shown in the following section.

5.5. Stage E

In stage E, shrinking bifurcation diagrams are disconnected at certain r_m and separated into two parts. One is said to be the survivor that will remain in stage F, and the other is called the vanisher that will disappear as slopes increase. After D1, the regions where period-2 gaits exist are disconnected at around $r_m = 1.104$ at a 2.60° slope as shown in Fig. 9(c) yielding a disconnected diagram like E1. The survivor is in the middle part that consists of period-1 and period-2 gaits, and the vanishers are at both ends, which include chaos. The disconnection occurs when a dominant eigenvalue stemmed from the mountainside of the eigenvalues hits the boundary of the unit circle as shown in Fig. 9. Stage E2 also has a left part as the survivor and a right part as the vanisher. The disconnection takes place at around $\ln r_m = 0$ unlike stage E1.

5.6. Stage F

In this last stage among six stages, the vanisher dwindles away at the edge between the survivor and the vanisher as slopes increase. At the end of stage F, the vanisher completely disappears. However, the survivor still remains and is a little

shrunk as shown in stages F1 and F2 of Table I. We note that the magnification of F1 is bigger than that of E1. After the extinction of the vanisher, bifurcation diagrams begin to expand again with increasing slopes. Expansion and contraction of bifurcation diagrams were observed after F2, but we were not able to classify diagrams from 4.96° to 5.20° as six stages.

6. Concluding Remarks

We categorized the bifurcation diagrams in passive walking with gait asymmetries into six stages in order to explain the transitions in detail. The process can be summarized by three qualitative changes. First, bubbles are created by period-doubling and period-remerging bifurcations leading to chaos. Second, when the bubbles are full of chaos, period remerged parts are instantly discarded. Third, period doubled parts also fade away after being disconnected. These changes are repeated from stage A2, but the difference is that stage F2 still has one of the period doubled parts, including chaos as a survivor.

The first qualitative change corresponds to stage B. Once chaos appears, it grows in stage C. The second qualitative change removes some parts of chaos in stage D. The third qualitative change described in stages E and F also removes chaos. It should be addressed that the second and the third changes regarding the extinction of chaos will never be recognized from a single bifurcation diagram drawn by one bifurcation parameter. One more bifurcation parameter shows us many bifurcation diagrams and enables us to examine the transitions between them.

In summary, we have investigated the effect of gait asymmetries on passive dynamic walking. For system modeling, we have proposed the concept of the composite hybrid systems. The ground slope and the mass ratio of right leg to left leg are used as two bifurcation parameters to reveal the consecutive bifurcation diagrams, which can be grouped into six stages. The first three stages are expanding, and the other three of them are contracting. We verified that period-doubling, period-remerging, and saddle-node bifurcations are exhibited in passive dynamic walking. In addition, we have discovered that chaos disappears through two qualitative changes after which the six stages are repeatedly observed. Furthermore, the same six stages appear even if we use another bifurcation parameter such as the length ratio of right leg to left leg instead of the mass ratio.

Acknowledgments

This research was partially supported by the Truchard Foundation, Austin, TX, and by the National Science Foundation Grant CMMI-0856368.

References

1. S. Aoi and K. Tsuchiya, "Bifurcation and chaos of a simple walking model driven by a rhythmic signal," *Int. J. Non-Linear Mech.* **41**(3), 438–446 (2006).
2. F. Asano and Z.-W. Luo, "Pseudo Virtual Passive Dynamic Walking and Effect of Upper Body as Counterweight," *Proceedings of IEEE/RSJ International Conference on Intelligent Robots Systems*, Nice, France (2008) pp. 2934–2939.
3. F. Asano and Z.-W. Luo, "On Efficiency and Optimality of Asymmetric Dynamic Bipedal Gait," *Proceedings of IEEE International Conference on Robotics Automation*, Kobe, Japan (2009) pp. 1972–1977.
4. M. Bier and T. C. Bountis, "Remerging feigenbaum trees in dynamical systems," *Phys. Lett. A* **104**(5), 239–244 (1984).
5. A. Ephanov and Y. Hurmuzlu, "Generating pathological gait patterns via the use of robotic locomotion models," *J. Technol. Health Care* **10**, 135–146 (2002).
6. M. J. Feigenbaum, "Quantitative universality for a class of nonlinear transformations," *J. Stat. Phys.* **19**(1), 25–52 (1978).
7. M. Garcia, A. Chatterjee, A. Ruina and M. Coleman, "The simplest walking model: Stability, complexity and scaling," *ASME J. Biomech. Eng.* **120**, 281–288 (1998).
8. A. Goswami, B. Espiau and A. Keramane, "Limit Cycles and Their Stability in a Passive Bipedal Gait," *Proceedings of IEEE International Conference on Robotics Automation*, Vol. 1, Minneapolis, MN (1996) pp. 246–251.
9. A. Goswami, B. Thuilot and B. Espiau, "Compass-Like Biped Robot. Part I: Stability and Bifurcation of Passive Gaits," *INRIA Technical Report* no. 2996 (INRIA, Grenoble, France. 1996).
10. A. Goswami, B. Thuilot and B. Espiau, "A study of the passive gait of a compass-like biped robot: Symmetry and chaos," *Int. J. Robot. Res.* **17**(12), 1282–1301 (1998).
11. J. Guckenheimer and P. Holmes, *Nonlinear Oscillations, Dynamical Systems, and Bifurcations of Vector Fields* (Springer-Verlag, New York, 1986).
12. Y. Harata, F. Asano, K. Taji and Y. Uno, "Efficient Parametric Excitation Walking with Delayed Feedback Control," *Proceedings of IEEE/RSJ International Conference on Intelligent Robots Systems*, St. Louis, MO (2009) pp. 2934–2939.
13. R. C. Hilborn, *Chaos and Nonlinear Dynamics: An Introduction for Scientists and Engineers* (Oxford University Press, New York, 2000).
14. G. W. Howell and J. Baillieul, "Simple Controllable Walking Mechanisms which Exhibit Bifurcations," *Proceedings of IEEE Conference on Decision Control*, Tampa, FL (1998) pp. 3027–3032.
15. C. S. Hsu, *Cell-to-Cell Mapping: A Method of Global Analysis for Nonlinear Systems* (Springer-Verlag, New York, 1987).
16. Y. Hurmuzlu and G. Moskowitz, "The role of impact in the stability of bipedal locomotion," *Dyn. Stab. Syst.* **1**(3), 217–234 (1986).
17. M. J. Kurz and N. Stergiou, "Hip actuations can be used to control bifurcations and chaos in a passive dynamic walking model," *ASME J. Biomech. Eng.* **129**(2), 216–222 (2007).
18. T. McGeer, "Passive dynamic walking," *Int. J. Robot. Res.* **9**(2), 62–82 (1990).
19. S. Mochon and T. A. McMahon, "Ballistic walking," *J. Biomech.* **13**(1), 49–57 (1980).
20. S. Mochon and T. A. McMahon, "Ballistic walking: An improved model," *Math. Biosci.* **52**(3–4), 241–260 (1980).
21. J.-S. Moon and M. W. Spong, "Bifurcations and Chaos in Passive Walking of a Compass-Gait Biped with Asymmetries," *Proceedings of IEEE International Conference on Robotics Automation*, Anchorage, AK, (2010) pp. 1721–1726.
22. E. Ott, *Chaos in Dynamical Systems* (Cambridge University Press, New York, 1993).
23. E. Ott, C. Grebogi and J. A. Yorke, "Controlling chaos," *Phys. Rev. Lett.* **64**(11), 1196–1199 (1990).
24. T. S. Parker and L. O. Chua, *Practical Numerical Algorithms for Chaotic Systems* (Springer-Verlag New York, NY, 1989).
25. T. Shinbrot, C. Grebogi, E. Ott and J. A. Yorke, "Using small perturbations to control chaos," *Nature* **363**, 411–417 (1993).
26. M. W. Spong, S. Hutchinson and M. Vidyasagar, *Robot Modeling and Control* (Wiley, Hoboken, NJ, 2006).
27. S. H. Strogatz, *Nonlinear Dynamics and Chaos: With Applications to Physics, Biology, Chemistry, and Engineering* (Addison-Wesley, Reading, MA, 1994).
28. S. Suzuki and K. Furuta, "Enhancement of Stabilization for Passive Walking by Chaos Control Approach," *Proceedings of IFAC Triennial World Congress*, Vol. B, Barcelona, Spain (2002) pp. 133–138.